



# Precise Orbit Determination of LEO Satellite Using Onboard BDS-3 B1C/B2a Observations

Youcun Wang<sup>(✉)</sup>, Qile Zhao, and Kecai Jiang

GNSS Research Center, Wuhan University, Wuhan 430079, China  
youcunwang@whu.edu.cn

**Abstract.** The precise orbit determination (POD) of low earth orbit (LEO) satellites is always a hotspot topic in the field of satellite geodesy. Current gravity field determination, satellite altimetry, and remote sensing measurement depend crucially on the precise orbits of the spacecraft. BeiDou global navigation satellite system (BDS-3) is officially completed in 2020 and offers positioning, navigation, and timing (PNT) service for global users. The onboard BDS measurements from LEO satellites can be used for LEO POD and served as an effective supplement for BDS tracking geometry. In this study, the BDS-3 observations with B1C and B2a signals of HY-2D spacecraft are employed for reduced-dynamic POD. For superior orbit quality, the extended analytical model for solar radiation pressure (SRP) is used for LEO POD, and in-flight calibration of the LEO receiver antenna is carried out to improve the orbit precision. Two weeks of onboard BDS-3 observation were used to assess the BDS-based POD performance. For HY-2D satellite based on BDS-3 instruments, the capability of continuous tracking is at the global level, and almost all the epochs can have 5–7 usable BDS satellites. The mean root-mean-squared (RMS) of the phase residual obtained from the reduced-dynamic POD is 6.5 mm, and that of pseudorange residual is 1.28 m. The internal precision for the entire arc is in good agreement. Moreover, an orbit self-consistency of 0.94 cm, 0.76 cm, and 0.49 cm is displayed in the along-track, cross-track, and radial directions, respectively.

The 1.33 cm 3D RMS of the internal consistency is achieved for the reduced-dynamic orbits. A better than 2 cm RMS has been achieved in the Satellite Laser Ranging (SLR) validation for BDS-3-based LEO orbit solutions. These results could be used for the Chinese subsequent LEO satellite equipped with a BDS-3 receiver.

**Keywords:** BDS-3 · LEO satellite · Precise orbit determination · B1C/B2a · Orbit precision

## 1 Introduction

Low-Earth orbit (LEO) missions with a height of about 100 km to 2000 km above play an important role in marine environmental monitoring, gravity detection, earth magnetic field research, occultation atmospheric observations, and other scientific fields,

greatly expanding human understanding of the Earth. LEO missions take routine measurements tasks and depend crucially on precise orbit determination. On 10 August 1992, the TOPEX/POSEIDON mission started providing high-altimetry measurements with the uncertainty of 3–4 cm in radial direction [1], the precise orbit products based on spaceborne global positioning system (GPS) technology has been widely used in LEO missions. Subsequent Jason-1/2/3 series satellites and Sentinel-3 altimetry satellites [2, 3], orbit determination better than 1 cm in the radial direction is obtained. For the CHAMP, GRACE, GOCE, and GRACE-FO satellites used for gravity field inversion [4–7], reduced-dynamic POD result of 2–3 cm precision can be achieved based on GPS observations.

The Beidou-3 (BDS-3) global navigation satellite system (GNSS) designed by China was officially completed in 2020, which together with other global navigation satellite systems provides positioning, navigation, and timing services to global users. The onboard BDS-3 receiver can provide continuous global tracking observations for LEO missions and support the BDS-3-based precise orbit determination for LEO missions.

HaiYang-2D (HY-2D) is the fourth satellite of the Chinese marine dynamic environment mission, which was launched on 19 May 2021 into LEO of 66 inclination, with an altitude of about 957 km. The major objective of the HY-2D is to monitor and investigate the marine environment. It carries various instruments, including a Ku/C-band altimeter, a scatterometer, and a microwave imager. A less than 3 cm RMS in the radial orbit component is officially specified for the HY-2D POD. To support this goal, the HY-2D spacecraft hosts a POD package, including an onboard GPS/BDS-3 receiver, a Doppler Orbitography, and Radiopositioning Integrated by Satellite (DORIS) instrument, and a laser retroreflector (LRR).

Within this study, the performance of BDS-3 observation from HY-2D is analyzed, and the potential of BDS-3 based POD for LEO satellites is assessed. For superior orbit product, the extended analytical solar radiation pressure (SRP) model [8] is suggested, and in-flight calibration of the BDS-3 antenna is performed for HY-2D POD. The phase residuals, orbit overlap comparisons, empirical parameters, and SLR validation are applied as a reasonable index for evaluating orbit quality. The results from HY-2D could be used for continued LEO missions equipped onboard the BDS-3 receiver.

## 2 HY-2D POD Package and BDS-3 Instrument

To support high-precision orbit, the HY-2D spacecraft hosts a POD package with dual-frequency and Combined GPS/BDS-3 receiver, DORIS equipment, and SLR (Satellite Laser Ranging) LRR. The onboard GPS/BDS-3 receiver supports frequencies that cover the L1/B1C band, the L2 band, and the B2a band. For BDS-3 signals, the 10 tracking channels are used for B1C and B2a frequencies which offer codes and carrier phase observations. Considering that the hardware processing capability of the onboard platform currently only dual-frequency single-system observation is supported. The onboard dual-frequency BDS-3 observations are in the test phase. For assessment of BDS-3 based LEO POD, the onboard B1C/B2a measurements from HY-2D are used for POD. The performance of BDS-3 based orbit solution is analyzed through phase residuals, overlap comparison, and SLR validation.

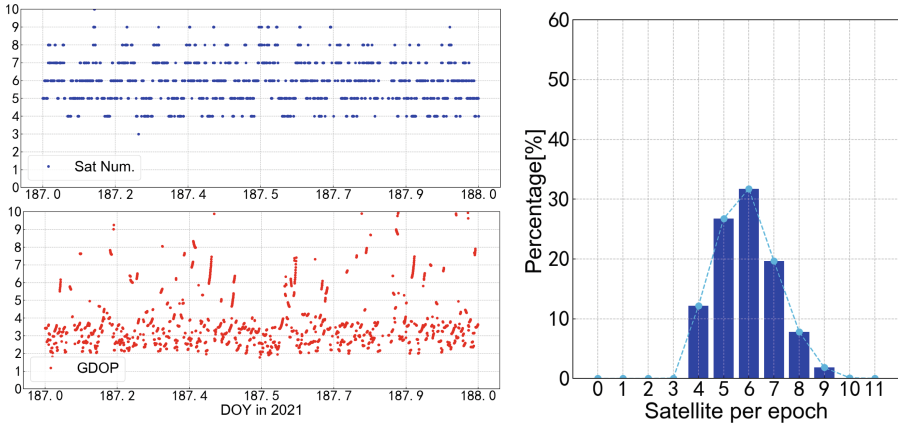


**Fig. 1.** The number of visible satellites and GDOP based on B1C/B2a observations for HY-2D

The continuous tracking capability of the satellite platform is an important prerequisite for LEO POD, and a wealth of observations for satellites add strong constraints for final orbit solutions. Currently, the BDS-3 (July 2020) has the functions of providing positioning, navigation, and timing for global users. The visibility of observations for HY-2D is shown in Fig. 1. The results indicated that 5–7 navigation satellites almost can be tracked during the entire arc, and the average level of GDOP is 4.9. To further analyze the global tracking observations based on the BDS-3, the grid observed BDS-3 satellite numbers along the HY-2D ground tracks from DOY 186/2021 to 199/2021 are illustrated in Fig. 2. In general, the performance of BDS-3 is further assessed through the LEO platform.

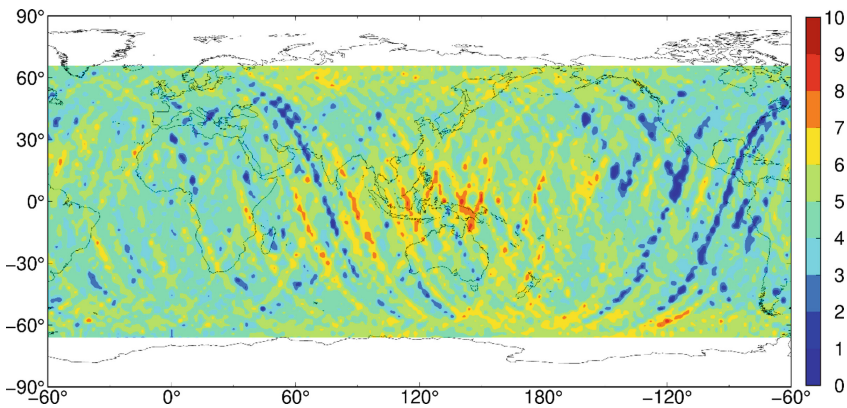


**Fig. 2.** Number of observed BDS-3 satellites per epoch for HY-2D

### 3 POD Scheme

#### 3.1 POD Data and Models

The HY-2D reduced-dynamic POD solutions are presented in this article, and the Position And Navigation Data Analyst (PANDA) software tools [9], which are developed by GNSS Research Center of Wuhan University, is used for GNSS high precision processing. The consecutive 30-h arc, which offers a 6-h overlap, is employed for HY-2D POD. The 30 s sampling of BDS-3 observations is consistent with standard IGS clock products. The summary of dynamical models and data sets is given in Table 1, and the reduced dynamic method and processing strategies are described in Jing-Nan and Mao-Rong [9].

**Table 1.** The employed models and processing standards of HY-2D satellite

Model	Description
<i>GNSS Measurements</i>	
BDS-3 Observation	Undifferenced ionosphere-free code and carrier phase combinations based on B1C/B2a
Interval and arc length	30 s and 30 h
BDS-3 orbit and clocks	WHU precise products [10]
GNSS satellite PCO & PCV	IGS ATX models [11, 12]
HY-2D attitude	Quaternions (measured)
HY-2D PCO & PCV	Corrections from in-flight calibration
<i>Dynamic model</i>	
Earth gravity	EIGEN_6C (120 × 120) [13]
Solid Earth and pole tides	IERS 2003 conventions [14]
Ocean Tides	FES 2004 (30 × 30) [15]
N-body disturbance	JPL DE405
Relativity	IERS 2003 conventions
Solar radiation pressure	16-plate macro-model, radiation pressure coefficients (VIS and IR) [8]
Atmospheric drag	16-plate macro-model, atmospheric density model adopting DTM-2013
Empirical acceleration	Piecewise periodic acceleration
<i>Estimated parameters</i>	
Initial state	Position and velocity at the initial epoch
Receiver clock offset	Each epoch as white noise
Phase ambiguities	Each continuous tracking arc as afloat

(continued)

**Table 1.** (continued)

Model	Description
Solar radiation coefficients	Scale factor for daily arcs
Drag coefficients	Scale factor per 120-min
Empirical acceleration	Amplitudes of periodic accelerations per 120-min in along-track and cross-track
<i>SLR validation</i>	
Station coordinates	SLRF2014 (v20/04/28) [16]
Tropospheric delay	Mendes and Pavlis [17]
Ocean tide loading	FES 2004 [15]
Relativity	IERS 2003 conventions

The reduced-dynamic POD of LEO satellites is calculated based on precise prior models. The orbit solution is affected by the error of the GNSS observation, but the accuracy of the dynamical model is the key for the precise orbit determination of the satellite. For LEO satellite missions with altitude above 800 km, solar radiation pressure (SRP) easily surpassed drag. For altimetry satellites with orbital altitudes around 1000 km, such as JASON-1/2/3 and HY2-A/B/C satellites [2, 18, 19], the solar radiation pressure is the main source of non-conservative force of the satellites. Therefore, the accurate modeling of SRP is required for precise orbit solutions. The SRP is closely related to the surface materials of satellites and the space environment [8]. The time-dependent radiation data products are used for removing systematic errors [8]. Details of this concept and the implementation of the physical radiation pressure model are described in Vielberg and Kusche [8].

The location is typically provided by the spacecraft manufacturer, with a nominal precision of millimeters or better, but the experience of past geodetic missions has shown that there may be inconsistencies at the level of 2–3 cm [3, 18, 19]. Considering the difference between the space environment of the satellite and the ground test scenario, offset calibration of the antenna phase center and empirical phase center variations (PCV) corrections were performed for HY-2D POD.

In this study, the direct approach is used to introduce the phase center offset (PCO) parameters into the observation equation for adjustment solution, and the estimation of PCV is obtained by the post-facto residual approach [20]. The reference values for the position of Center-of-mass (CoM), GNSS receiver antenna, LRR, and PCO estimation are given in Table 2.

**Table 2.** Locations for GNSS receiver, LRR, and CoM in the body-fixed coordinate system

Item	Reference (x, y, z) (mm)	Notes
CoM location	(+1332.00, -8.60, +3.40)	May 2021
GNSS antenna location	(+347.29, -175.14, -1372.68)	GNSS-antenna-b
LRR location	(+312.810, -215.68, +985.98)	
GNSS antenna PCO	(+0.0, +0.0, +20.0)	Valid for ionosphere-free phase combination

## 4 POD Results and Analysis

To further investigate the accuracy of BDS-based POD orbit, the onboard BDS-3 data of HY-2D from 186 days in 2021 to 199 days in 2021 are used for reduced-dynamic orbit determination. The precision of the reduced-dynamic HY-2D orbits using BDS-3 B1C/B2a observations was confirmed by observations residuals, orbit comparisons, and SLR analysis. The detailed validation and POD results are discussed in this section.

### 4.1 Observation Residuals

The residual of the phase observation obtained from POD is a reasonable index of evaluating the orbit quality. Large or abnormal values usually mean poor parameter estimation in the POD. In general, the residuals of observations provide an internal means of assessing the precision of the orbit.

The daily RMS of PC and LC residuals for B1C/B2a data from HY-2D POD are shown in Fig. 3. The mean Total Electron Content Unit (TECU) (see Fig. 3) obtained from the Center for Orbit Determination in Europe (CODE) [21, 22] is employed to characterize the ionospheric delay and solar activity. The average RMS of the LC and PC residuals from reduced dynamic POD are approximately 6.5 mm and 12.8 dm, respectively. Except for some abnormal areas, the coincidence accuracy within the observation residuals is maintained at about 10 mm.

To further analyze the results of the phase residuals based on BDS-3, Fig. 4 shows the global grid distribution of the phase residuals. Except for a few abnormal regions, the observation residuals are maintained at about 10 mm. The residuals for the entire arc section are in good agreement.

### 4.2 Offset Calibration of BDS-3 Antenna

In this study, the azimuth- and zenith/nadir-dependent PCV correction of HY-2D is obtained by the residual approach [20]. The 14-days carrier phase residuals from LEO reduced-dynamic POD are used. The HY-2D satellite performed an attitude flipping during the 14-day arc. Figure 5 shows the variation in the geometric distribution of BDS-3 data points in the antenna reference frame before and after the HY-2D attitude flipping.

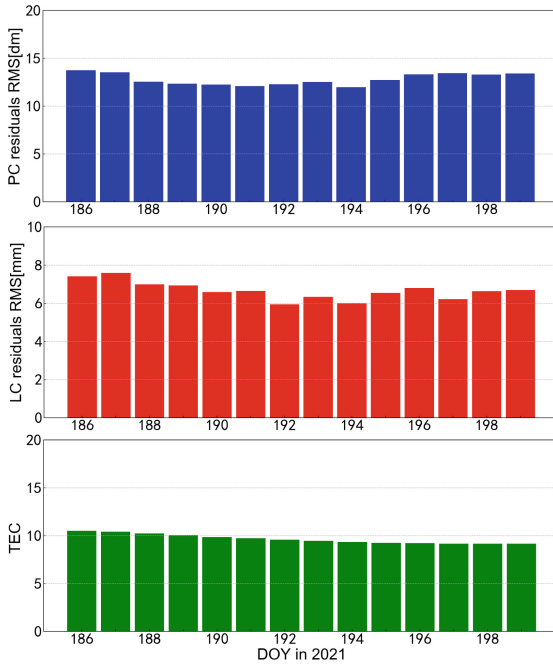


**Fig. 3.** Daily RMS of the ionosphere-free code range linear combination (PC) (top) and phase linear combination (LC) (middle) residuals for B1C/B2a observations

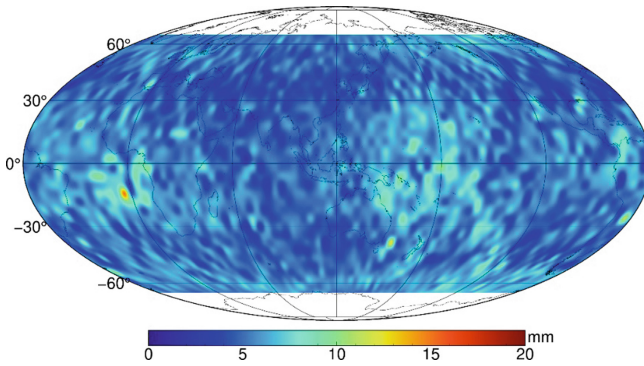


**Fig. 4.** The global grid results of phase residuals from HY-2D POD based on BDS-3 observations

The residuals with uniform coverage are an important prerequisite for reasonable PCV estimation, The phase residuals over a 14-day data set are used for PCV estimation, and the PCV map is shown in Fig. 6. Peak values of HY-2D BDS-3 PCV amount to 15 mm, and typical phase corrections are substantially smaller.

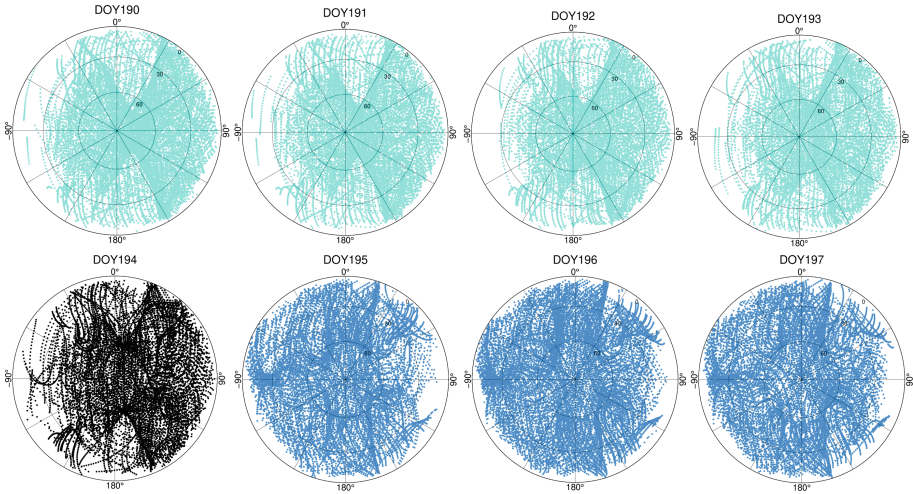


**Fig. 5.** Distribution of BDS-3 phase observations in the antenna frame. The light blue dot and dark blue dot (before and after the yaw flip), the black dot (when the satellite makes a yaw flip). The azimuth of  $0^\circ$  points to the  $+x$ -axis of the satellite body and the elevation of  $90^\circ$  is the antenna boresight.

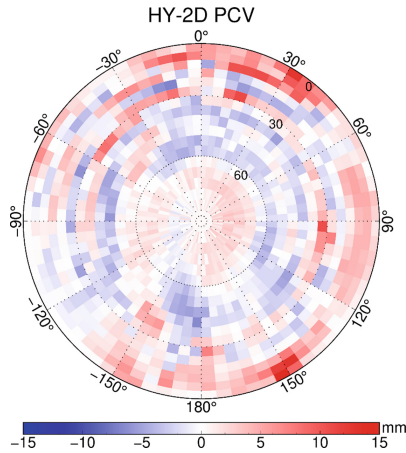


**Fig. 6.** Polar plot of phase variations for the HY-2D antenna is derived from phase residuals in POD.

### 4.3 Overlap Comparison

The overlap difference is widely used to assess the internal precision of the reduced-dynamic orbit. The orbit difference of two consecutive orbit solutions in the common arcs was adopted to evaluate the consistency of the POD.

The RMS of daily overlap difference for HY-2D is shown in Fig. 7. The 1.33 cm 3D RMS is achieved in HY-2D reduced-dynamic orbit, and a better than 0.5 cm RMS consistency in the radial direction is supported. There is no noticeable dependency on



the  $\beta$ -angle for HY-2D POD. The orbit comparison with the DORIS-based product is shown in Fig. 7. The mean RMS of orbit differences of 1.2 cm is obtained in the radial direction. The CNES orbit products are available at <ftp://ftp-access.aviso.altimetry.fr/geophysical-data-record/doris>.

When the PCV model is considered in the POD, a noticeable improvement occurs in the self-consistency for the HY-2D (see Fig. 8). Compare to the solutions without PCV, the RMS of for 3D position overlap difference decreased by 9.5% for the orbit solution with PCV, and the orbit accuracy has been improved to varying degrees in three directions.

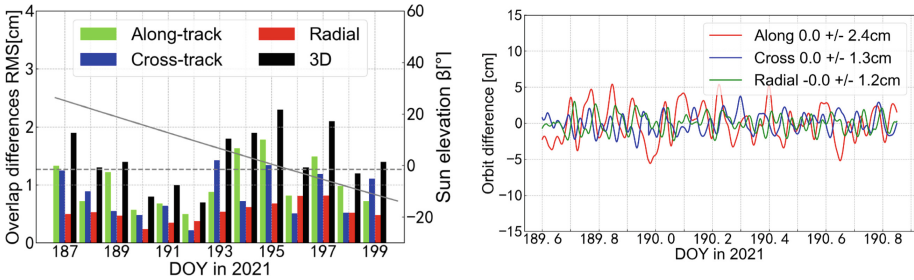


**Fig. 7.** Daily RMS of the overlap differences in along-track (green), cross-track (blue), radial (red) and position for HY-2D POD (left). The  $\beta$ -angle of HY-2D is shown in gray line, and the dotted horizontal line marks the  $\beta$ -angle threshold for yaw flipping. The orbit differences between the BDS3-based orbit solution and CNES orbit solution for HY-2D (right).

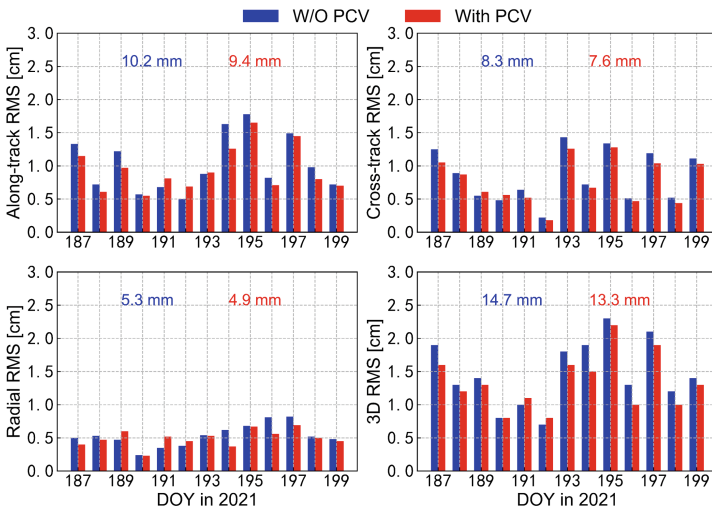


**Fig. 8.** Comparison of overlap difference for HY-2D POD using without PCV (blue) and with PCV (red) calibration

### 4.4 Empirical Accelerations

The reduced-dynamic POD of HY-2D makes use of empirical parameters for individual forces, and empirical accelerations to compensate for modeling deficiencies. The magnitude of residual accelerations suggests an indicator of dynamical forces’ accuracy and orbit quality. In this study, the auxiliary Angle formula is used to calculate the magnitude of the empirical acceleration, and the scale factor for SRP and the Sun’s elevation  $\beta$  above the orbital plane are shown in Fig. 9.

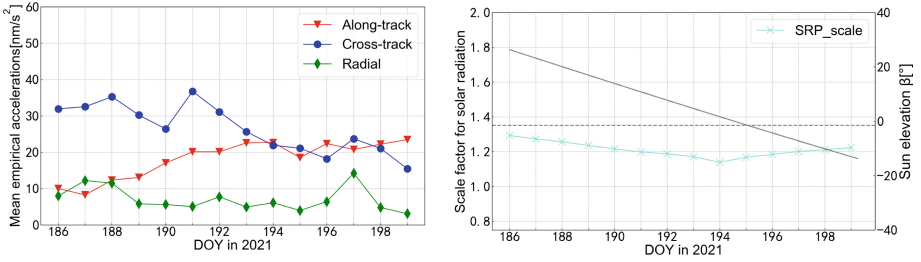


**Fig. 9.** The left is daily mean values of empirical acceleration in radial, along-track, and cross-track directions. The right is the scale factor for solar radiation pressure (SRP) and  $\beta$  angle

The magnitude of empirical acceleration in along-track and normal directions amounts to 20–30, and the radial direction is the smallest, which is substantially maintained at 10. Figure 9 depicts the scale factor of SRP Satellite and  $\beta$  angle of HY-2D. A slight increase of variability from 0.1 to 0.2 for HY-2D is observed. The scale factor is correlated with the  $\beta$  angle of HY-2D which determines the varying Sun illumination. In short, the empirical acceleration and scale parameters are in reasonable agreement.

### 4.5 SLR Validation

SLR measurements are used as a key technique for independent validation of the GNSS-based orbits for LEO POD [23, 24]. The HY-2D is equipped with an SLR LRR to provide an observation guarantee for its POD and orbit validations. The 1343 normal points from 12 SLR stations are selected. In all computations, observations above the 8 elevations were employed, and an outlier threshold of 15 cm was used (0.51% of the SLR normal point were rejected).

The SLR residuals of reduced-dynamic orbit solution are shown in Fig. 10. RMS residuals of 21.5 and 19.7 mm are obtained for orbit solution without (red) and with (blue) PCV corrections. Compare to orbits without PCV corrections, the SLR validation exhibit the 8.3% reduction in the RMS residuals.

Considering that the SLR data quality is related to the elevation angle of the SLR station [25, 26], SLR residuals concerning the elevation angles are shown in Fig. 11. The overall mean bias is improved from  $-7.8$  mm to  $-6.4$  mm for the solution with PCV. Above all, the PCV map of the HY-2D BDS-3 can well describe the variation in the instantaneous phase center of the receiver antenna, and the orbit determination accuracy has been improved after correction.

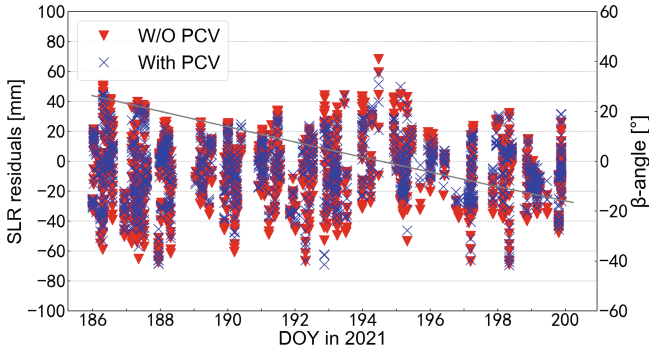


**Fig. 10.** SLR residuals of HY-2D POD based on BDS-3 observations

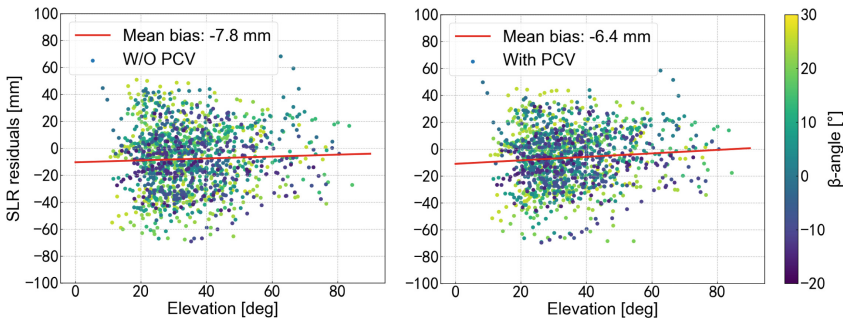


**Fig. 11.** The SLR residuals as a function of the elevation angle are shown with a fitted trend line (in red). The left is the solution without PCV and the right is the solution with PCV.

## 5 Summary and Conclusions

This article focuses on the BDS-3 based LEO POD, and HY-2D is the first altimetry mission using the BDS-3 receiver for precise orbit determination. For the HY-2D mission, a two-week data period is covered in this study, and the achievable orbit precision from reduced-dynamic POD was assessed. Compare to standard analytical solar radiation pressure, time-dependent radiation data and dependency of the wavelength are considered to yield an improved SRP model in POD processing. Similar to other LEO missions, a systematic error in nominal BDS-3 antenna phase center and phase variations can be observed for HY-2D. A 20-mm offset in the PCO z-component is adopted in this study and a map of PCV as a function of elevation and azimuth were applied in HY-2D POD.

The phase residuals, overlap differences, and independent verification of SLR measured normal points are used for resulting POD accuracy. The average consistency for the reduced-dynamic POD solution using BDS-3 observations is at the 1.33 cm 3D RMS. The uncertainty of better than 2 cm is achieved in independent SLR validation for BDS-3 based orbits. The BDS-3 based precise orbit determination for LEO missions with centimeter-level precision is confirmed through the results of HY-2D POD.

This contribution could be used for following low Earth orbit missions using the BDS-3 receiver.

## References

1. Tapley, B.D., Ries, J.C., Davis, G.W., et al.: Precision orbit determination for Topex/Poseidon. *J. Geophys. Res. Oceans* **99**(C12), 24383–24404 (1994)
2. Flohrer, C., Otten, M., Springer, T., et al.: Generating precise and homogeneous orbits for Jason-1 and Jason-2. *Adv. Space Res.* **48**(1), 152–172 (2011)
3. Montenbruck, O., Hackel, S., Jäggi, A.: Precise orbit determination of the Sentinel-3A altimetry satellite using ambiguity-fixed GPS carrier phase observations. *J. Geodesy* **92**(7), 711–726 (2018)
4. Tapley, B.D., Bettadpur, S., Ries, J.C., et al.: GRACE measurements of mass variability in the Earth system. *Science* **305**(5683), 503–505 (2004)
5. Kang, Z., Tapley, B., Bettadpur, S., et al.: Precise orbit determination for the GRACE mission using only GPS data. *J. Geodesy* **80**(6), 322–331 (2006)
6. Kornfeld, R.P., Arnold, B.W., Gross, M.A., et al.: GRACE-FO: The Gravity Recovery and Climate Experiment Follow-On Mission [J]. *Journal Of Spacecraft And Rockets* **56**(3), 931–951 (2019)
7. Bock, H., Jäggi, A., Beutler, G., et al.: GOCE: precise orbit determination for the entire mission. *J. Geodesy* **88**(11), 1047–1060 (2014)
8. Vielberg, K., Kusche, J.: Extended forward and inverse modeling of radiation pressure accelerations for LEO satellites. *J. Geodesy* **94**(4), 1–21 (2020)
9. Jing-Nan, L., Mao-Rong, G.: PANDA software and its preliminary result of positioning and orbit determination. *Wuhan Univ. J. Nat. Sci.* **8**(2), 603–609 (2003)
10. Zhao, Q., Guo, J., Wang, C., et al.: Precise orbit determination for BDS satellites. *Satellite Navig.* **3**(1), 1–24 (2022)
11. Rebischung, P., Schmid, R.: IGS14/igs14.atx: a new framework for the IGS products; proceedings of the AGU Fall Meeting Abstracts, F (2016)
12. Schmid, R., Dach, R., Collilieux, X., Jäggi, A., Schmitz, M., Dilssner, F.: Absolute IGS antenna phase center model igs08.atx: status and potential improvements. *J. Geodesy* **90**(4), 343–364 (2015)
13. Shako, R., Förste, C., Abrikosov, O., Bruinsma, S., Marty, J.-C., Lemoine, J.-M., Flechtner, F., Neumayer, H., Dahle, C.: EIGEN-6C: a high-resolution global gravity combination model including GOCE data. In: Flechtner, F., Sneeuw, N., Schuh, W.-D. (eds.) *Observation of the System Earth from Space - CHAMP, GRACE, GOCE and future missions: GEOTECHNOLOGIEN Science Report No. 20*, pp. 155–161. Springer Berlin Heidelberg, Berlin, Heidelberg (2014). [https://doi.org/10.1007/978-3-642-32135-1\\_20](https://doi.org/10.1007/978-3-642-32135-1_20)
14. Petit, G., Luzum, B.: Bureau International des Poids et mesures sevres (france) (2010)
15. Lyard, F., Lefevre, F., Letellier, T., et al.: Modelling the global ocean tides: modern insights from FES2004. *Ocean Dyn.* **56**(5), 394–415 (2006)
16. ILRS: SLRF2014 station coordinates (2020)
17. Mendes, V.B., Pavlis, E.C.: High-accuracy zenith delay prediction at optical wavelengths. *Geophys. Res. Lett.* **31**(14), 1–5 (2004)
18. Wang, Y.C., Li, M., Jiang, K.C., et al.: Precise orbit determination of the Haiyang 2C altimetry satellite using attitude modeling. *GPS Sol.* **26**(1), 1–14 (2022)
19. Wang, Y., et al.: Reduced-dynamic precise orbit determination of Haiyang-2B altimetry satellite using a refined empirical acceleration model. *Remote Sensing* **13**(18), 3702 (2021)

20. Jäggi, A., Dach, R., Montenbruck, O., et al.: Phase center modeling for LEO GPS receiver antennas and its impact on precise orbit determination. *J. Geodesy* **83**(12), 1145–1162 (2009)
21. Dow, J.M., Neilan, R.E., Rizos, C.: The international GNSS service in a changing landscape of global navigation satellite systems. *J. Geodesy* **83**(3–4), 191–198 (2009)
22. Schaer, S., Villiger, A., Arnold, D., Dach, R., Prange, L., Jäggi, A.: The CODE ambiguity-fixed clock and phase bias analysis products: generation, properties, and performance. *J. Geodesy* **95**(7), 1–25 (2021)
23. Pearlman, M.R., et al.: The ILRS: approaching 20 years and planning for the future. *J. Geodesy* **93**(11), 2161–2180 (2019)
24. Guo, J.Y., Wang, Y.C., Shen, Y., et al.: Estimation of SLR station coordinates by means of SLR measurements to kinematic orbit of LEO satellites. *Earth Planets Space* **70**(1), 201 (2018)
25. Drożdżewski, M., Sośnica, K.: Tropospheric and range biases in Satellite Laser Ranging. *J. Geodesy* **95**(9), 1–18 (2021)
26. Strugarek, D., Sośnica, K., Zajdel, R., Bury, G.: Detector-specific issues in Satellite Laser Ranging to Swarm-A/B/C satellites. *Measurement* **182**, 109786 (2021)